Silver nanoparticles against acute hepatopancreatic necrosis disease (AHPND) in shrimp and their depuration kinetics

Maribel Maldonado-Muñiz[1] · Carlos Luna[2] · Raquel Mendoza-Reséndez[2] · Enrique Díaz Barriga-Castro[3] · Sonia Soto-Rodriguez[4] · Denis Ricque-Marie[1] · Lucia Elizabeth Cruz-Suarez[1]

Abstract

Ag-based nanoparticles (NPs) were successfully produced through green synthesis using an aqueous extract from the cultivated seaweed *Ulva clathrata* as the reducing and stabilizing agent. The biosynthesized NPs had spherical to polymorphic shapes with an average size of 9.5 nm. Microstructural and compositional studies revealed that these particles contained face-centred cubic crystallites of metallic Ag and AgCl. Characteristic peaks in the Fourier-transform infrared spectrum (FTIR) and Raman studies revealed the presence of functional bioactive metabolites from the seaweed extract, such as proteins, polysaccharides, and polyphenols, which are responsible for forming and stabilizing Ag/AgCl NPs. The biosynthesized Ag/AgCl NPs exhibited an important in vitro antibacterial effect against three *Vibrio parahaemolyticus* strains isolated from farmed shrimp affected with acute hepatopancreatic necrosis disease (AHPND) in northwestern Mexico. *Litopenaeus vannamei* shrimp were exposed for 7 days to feeds supplemented with Ag/AgCl NPs at 10, 100, 1000, or 10,000 ppm (Ag nominal dietary concentrations). Dietary NP supplement did not affect shrimp survival, growth, or feed conversion ratio, but high concentrations (1000 and 10,000 ppm) decreased the hepatosomatic index significantly. The short-term consumption of Ag/AgCl NPs produced a significant dose-dependent bioaccumulation of Ag in the hepatopancreas and to a lesser extent in the cuticle, while bioaccumulation in the muscle was not significant. The depuration study confirmed a fast Ag assimilation in shrimp's hepatopancreas and showed a fast depuration rate in the hepatopancreas as well.

Keywords Antibacterial activity · Green seaweed · Green synthesis · *Litopenaeus vannamei* · *Vibrio parahaemolyticus*

✉ Lucia Elizabeth Cruz-Suarez
lucia.cruzsr@uanl.edu.mx

[1] Facultad de Ciencias Biologicas (FCB), Universidad Autonoma de Nuevo Leon (UANL), Av. Universidad S/N, 66455 San Nicolás de los Garza, Nuevo Leon, Mexico

[2] Facultad de Ciencias Fisico Matematicas (FCFM), Universidad Autonoma de Nuevo Leon (UANL), Av. Universidad S/N, 66455 San Nicolas de los Garza, Nuevo Leon, Mexico

[3] Centro de Investigacion en Quimica Aplicada (CIQA), Blvd. Enrique Reyna Hermosillo, No. 140, 25294 Saltillo, Coahuila, Mexico

[4] Centro de Investigación Alimentacion y Desarrollo, Av. Sabalo-Cerritos s/n, Estero del Yugo, 82000 Mazatlan, Sinaloa, Mexico

Introduction

Shrimp farming is one of the most important aquaculture economic activities in the world, and this activity generates important economic benefits. Mexico is one of the main exporters to important international markets such as USA, Vietnam and France (Conapesca 2017). Newly emerged penaeid shrimp diseases caused by opportunistic pathogens such as *Vibrio* are producing economic losses in Mexico and worldwide (Aguirre-Guzmán et al. 2004). In 2009, the first cases of acute hepatopancreatic necrosis disease (AHPND), previously referred to as early mortality syndrome (EMS), appeared in China, Vietnam, Thailand and Malaysia. Since 2013, high mortalities (40 to 100% in the first 35 days of shrimp farming) caused by AHPND have been also reported in Mexico and Central American countries. This disease is caused by certain pathogenic strains of *Vibrio parahaemolyticus* and is characterized by a severe atrophy of the shrimp's hepatopancreas (HP) (Joshi et al. 2014; Yang

et al. 2014; Soto-Rodriguez et al. 2015). To address these issues, several antimicrobial agents were assayed. However, these failed to completely satisfy aquaculture needs as *Vibrio* species developed resistance to some of these treatments (Sirvakumar et al. 2014; OIE 2014). The use of antibiotics to control *Vibrio* strains in shrimp aquaculture is not allowed in most of the countries (Defoirdt et al. 2011). Therefore, it is necessary to develop alternative methods for the effective control of *Vibrio* strains in shrimp production. In the face of this problem, silver nanoparticles (AgNPs) are a promising alternative because of their unique chemical and antimicrobial properties (Rai et al. 2009; Swain et al. 2014; Singh et al. 2015; Sivaramasamy and Zhiwei 2016).

Different varieties of microorganisms and plant extracts have been used in the last years for the production of metallic nanoparticles with low or no toxicity. These procedures have been called 'green synthesis' or 'green chemistry' (Dehnavi et al. 2013). Green synthesis provides advantages over physical methods and conventional chemical synthesis of nanomaterials because it produces NPs with inexpensive and energy-efficient processes that have little to no impact on the environment and human health. In addition, these processes can be easily scalable and also do not require the use of high pressure, energy, temperature, or toxic chemicals (Abdel-Raouf et al. 2017).

Seaweeds are commercially-important, renewable, marine living resources (Kumar et al. 2012) with biologically-active compounds that have activities against pathogens such as viruses, bacteria and fungi (Ibañez et al. 2012). Scientists have researched the green synthesis of gold and silver nanoparticles using several seaweed species and obtained nanoparticles with sizes averaging from 5 to 200 nm, a high synthesis rate, and an excellent colloidal stability. The phytochemicals present in seaweed extracts such as carbohydrates, peptides, alkaloids, steroids, phenolics, saponins and flavonoids are responsible for the reduction and stabilization of nanoparticles (Rai et al. 2009; Prasad et al. 2013; Swain et al. 2014; Singh et al. 2015; Sivaramasamy and Zhiwei 2016; Vieira et al. 2016).

Ulva clathrata (Roth) C. Agardh is a green alga from the Ulvaceae family with a worldwide distribution, and it can be also produced by aquaculture. This seaweed has several applications in shrimp farming as a functional feed additive or as fresh food in co-culture with white shrimp *Litopenaeus vannamei*, allowing healthier shrimp and improved water quality (Cruz-Suarez et al. 2010, 2013; Laramore et al. 2018; Peña-Rodríguez et al. 2010). Cultivated *U.* could be a promising source of reduction agents for the synthesis of nanoparticles, which production would be then easily scalable.

Although two recent reports evidenced the efficacy of AgNPs in vivo (Morales-Covarrubias et al. 2016) and in vitro against AHPND-causing *V. parahaemolyticus* (Sivaramasamy et al. 2017), none had been synthetized with

seaweed extracts. Considering these antecedents, the aim of this study was to purify and characterize Ag-based NPs produced through green chemistry using an aqueous extract of cultivated *U. clathrata* (AEU), and to evaluate their in vitro antibacterial activity against three *V. parahaemolyticus* strains obtained from farmed shrimp affected with AHPND in north-western Mexico. In addition, this project sought to examine, through short-term dietary exposure experiments, the effects of Ag-based NPs on shrimp survival and growth, as well as the Ag bioaccumulation-distribution in different tissues along with its depuration kinetics.

Materials and methods

Chemical reagents Water sterile-filtered (W3500), silver nitrate (209139), resazurine sodium salt (R7017), and sodium chloride (V000106) were from Sigma-Aldrich (USA). The bacteriological mediums Tryptic Soy Agar (TSA), Tryptic Soy Broth (TSB), Mueller Hinton Agar (MHA), Mueller Hinton Broth (MHB) and Agar Agar (AA) were obtained from Difco (USA).

Seaweed *Ulva clathrata* (Roth) C. Agardh was cultivated on a large-scale system in a shrimp earthen pond in Sinaloa, Mexico. Details of production and processing conditions are reported by Peña-Rodríguez et al. (2011).

Bacterial strains *Vibrio parahaemolyticus* strains were obtained from laboratory culture collections at CIAD Mazatlan, Sinaloa, Mexico. Samples were isolated from the stomach and hepatopancreas of farmed shrimp affected with AHPND in northwestern Mexico. The molecular identification, characterization and pathogenicity of the bacterial isolates used in this work were reported by Soto-Rodriguez et al. (2015); *V. parahaemolyticus* strains M9-04 and M6-05 are classified as pathogenic, and M5-28 as non-pathogenic. Strains were maintained in cryopreservation (− 80 °C) until activated in TSB supplemented with 2% NaCl.

Preparation of aqueous extract of *Ulva* (AEU) Ten gram of seaweed powder was extracted with 200 mL of distilled hot water (90 °C) stirred constantly for 15 min and left to stand in darkness for 12 h before centrifugation (2500 rpm) for 15 min (IEC Centra MP4R, International equipment company, USA). The pellet was washed twice with 100 mL hot water at 90 °C. The soluble extracts were pooled and frozen at − 80 °C (ULT 1386-3-A14, Revco Scientific Inc., USA) for subsequent freeze-drying (Freezone Benchtop 6L, Labconco, USA).

Synthesis of NPs NPs were obtained through green synthesis with our patented method (Luna et al. 2015a, 2015b) by adding 100 mL AgNO$_3$ (1×10^{-3} M) aqueous solution to a

flask containing 170 mg AEU previously dissolved in 100 mL Sigma sterile-filtered water. The mixture was kept in constant magnetic stirring at room temperature for 48 h. The formation of NPs was confirmed by solution colour change. NPs were washed three times using absolute ethanol (ratio 1:3) as an antisolvent for precipitation assistance and centrifuged (10,000 rpm). Finally, the purified precipitate was re-dispersed using ultrasound (Ultrasonic cleaner 50HT, VWR International, USA) in Sigma sterile-filtered water for further characterization studies. Ag concentration was measured by atomic absorption spectroscopy (AAS) (ICE AAS 3500, ThermoScientific, UK) according to the AOAC method 990.08 (AOAC 1997) and was expressed in µg Ag mL^{-1}.

Characterization of NPs NPs presence in the brown purified colloidal sample were confirmed through UV-vis spectroscopy (Nicolet 60S, ThermoFisher Scientific, USA) analysis in the wavelength range of 300–1100 nm. Surface plasmon resonance (SPR) was observed for AgNPs. AEU without the addition of AgNO$_3$ solution was also analysed.

Crystal phases present in the sample were identified by powder X-ray diffraction (XRD) studies (X′Pert PRO diffractometer, Panalytical, USA) with Cu Kα (λ = 1.5418 Å) radiation. In this study, purified colloidal samples were dried at 50 °C overnight, obtaining dried samples in powder form. Values of the mean coherence length perpendicular to the crystallographic planes (200) of AgCl and (111) of metallic Ag, L$_{200,AgCl}$ and L$_{111,Ag}$, were estimated using the Scherrer equation (Luna et al. 2015a, 2015b)

$$L_{\mathrm{hkl}} = \frac{0.9\,\lambda}{\beta \cos\theta} \tag{1}$$

where λ is the X-ray wavelength, β is the broadening of the diffraction peak (after subtracting the instrumental broadening), and θ is the Bragg angle.

Particle morphology and size distributions of the biosynthesized samples were examined with transmission electron microscopy (TEM) using a microscope (TITAN 80–300 kV, FEI, USA) operated at 300 kV. To obtain more detailed information about the microstructural properties of the samples, high-resolution transmission electron microscopy (HRTEM) and selected-area electron diffraction (SAED) analyses were also carried out. Moreover, energy-dispersive spectrometry (EDX) measurements were performed with an EDS analyser attached to the TEM. For these studies, the colloidal sample was properly diluted with water and a drop was deposited onto a lacey-carbon copper grid and allowed to dry in ambient conditions in a free-powder area. No evidence of structural or chemical transformations of the samples was present during the TEM examination. Processing of TEM micrographs and analysis of HRTEM images by fast Fourier transforms (FFT) was carried out using the software Digital Micrograph 3.7.0 (Gatan Inc., USA).

FTIR and Raman studies were performed to identify the functional groups of the AEU responsible for the reduction of Ag$^+$ ions to Ag^0, and their stabilizing action on Ag-based nanoparticles. FTIR spectra (Nicolet 510 Fourier transform spectrometer, ThermoFisher Scientific, USA) were collected after diluting the specimen in KBr pellets in the wavenumber range of 500–4000 cm^{-1}. Raman spectra (HR800 UV Confocal Raman Microscope, Horiba Scientific, USA) were recorded across the range of 500–4000 cm^{-1} using a green laser (532.14 nm), working at 600 line mm^{-1}, × 100 objective, 20 mW, and 0.1-mm pinhole.

Antibacterial activity in vitro tests

Disc diffusion assay was performed on Mueller Hinton agar (MHA) plates plus 2% NaCl spread with 100 µL of each *V. parahaemolyticus* bacterial suspension (1 × 10^6 UFC mL^{-1}). Under aseptic conditions, filter paper discs (6 mm) were saturated with 20 µL of each stock solution test from AEU (50 µg dry extract mL^{-1}), Ag/AgCl NPs, AgNO$_3$ solution (50 µg Ag mL^{-1}) or distilled water (negative control), and were placed on MHA plates. The final concentration was 1 µg disc^{-1}. After 24 h of incubation at 29 °C, the inhibition zone (IZ) was measured with a digital Vernier (CD-6″CS, Mitotuyo Corp., Japan), and the IZ values were recorded as the average (mm) of two diameter measurements per disc taken in perpendicular directions. Triplicates of the assay were performed for each strain.

Microdilution broth assays were carried out according to Sarker et al. (2007) with certain modifications. Different concentrations (100, 50, 25, 12.5, 10, 8 and 6 µg Ag mL^{-1}) of Ag/AgCl NPs and AgNO$_3$ solution were prepared, and each one was added to four wells of sterile polystyrene 96-well microtiter plates (3370 Costar, USA). Additionally, 100 µL of Mueller Hinton broth (MHB) with 2% NaCl and 50 µL of each bacterial strain suspension (1 × 10^6 UFC mL^{-1}) were added to each well. Pure MHB with 2% NaCl, sterile water and bacterial suspension were used as a negative control, while sample blanks were the evaluated treatments and media without bacteria. After incubation at 29 °C for 20 h, 10 µL of 0.1% aqueous solution resazurine sodium salt were added and samples were incubated for four additional hours at the same temperature. Colour change was then assessed visually. Any colour changes from purple to pink or colourless were recorded as positive bacterial growth. The lowest concentration that produces a colour change was taken as the MIC value (Zhao and Stevens 1998). The lowest concentration at which no colour change occurred was registered to the MBC. Triplicates of the assay were performed for each strain.

Short-term evaluation in vivo tests Two different experiments were conducted to examine effects in survival and growth performance, tissue bioaccumulation-distribution and depuration of the Ag/AgCl NPs by short-term dietary exposure in shrimp. The experiments were performed according to OECD recommendations for acute toxicity in aquatic arthropods (OECD 2005) and dietary exposure bioaccumulation-distribution in fish (OECD 2012).

Supplemented feed preparation A commercial pelleted feed with 44% protein and 8% lipid contents (742 UANL, Nutrimar, Sinaloa, Mexico) was supplemented by aspersion with Ag/AgCl NPs stock solution in order to obtain Ag concentrations of 0, 10, 100, 1000 and 10,000 mg Ag kg^{-1}. Different Ag/AgCl NP stock solutions were diluted or concentrated in the same final volume of distilled water (40 mL) and sprayed on 100 g of feed previously weighed and placed in aluminium trays. Diets were mixed for 5 min to ensure complete homogenization. Finally, the feed was oven-dried at 50 °C for 1 h. The final Ag concentration in Ag/AgCl NP-supplemented feeds was quantified by AAS as described above.

Estimation of NP losses from diets The percentage of Ag/AgCl NPs lost from diets through leaching in seawater was estimated as described by Nieto-López et al. (2011) with certain modifications, including a correction in the % dry matter loss expression (%DML) for the marine salt absorbed by the immersed diets for 1 h in seawater (35 g L^{-1}, 28 °C). Ag content in leaching diets and in the water of each sample was determined by AAS and expressed as mg Ag kg^{-1} dry matter or mg Ag L^{-1} water.

Short-term acute toxicity and tissue distribution in vivo test The first in vivo test evaluated acute toxicity using behavioural, survival and growth performance parameters, and analysed tissue distribution of Ag/AgCl NPs after 7 days of feed consumption with low (0, 10 and 100 mg Ag kg^{-1}) and high (1000, 10,000 mg Ag kg^{-1}) dietary levels. During the experiment, 150 juvenile shrimp [*Litopenaeus vannamei* (Boone, 1931) provided by FITMAR, Sinaloa, Mexico (0.400 ± 0.02 g mean initial weight)] were randomly allocated in 15 rectangular fibreglass tanks of 10 L (10 shrimps per tank, five treatments and three replicates). Experimental tanks had constant individual aeration and were maintained daily with 100% manual exchange of artificial seawater (Pro Aquatics, Fritz Industrial Inc., Mesquite TX, USA) and natural conditions of photoperiod. Water temperature, salinity and pH, ammonia, nitrite, and dissolved oxygen contents were monitored daily and maintained under favourable limits for shrimp growth. The daily feed ration was 5% of total biomass per tank.

Acute toxicity parameters After 7 days of feeding shrimp with the different treatments, their behavioural effects were registered. Zootechnical parameters such as survival (%), weight gain (%) and feed conversion ratio (FCR) were calculated according to Cruz-Suarez et al. (2009).

Tissue sampling for acute toxicity test The hepatopancreas, cephalothorax cuticle and muscle from ten shrimps per treatment were dissected with tweezers before the beginning and at the end of the dietary exposure. The hepatopancreas for each shrimp was weighed individually, and the hepatosomatic index was determined using the formula shown in Eq. 2. The dissected shrimp samples of each tank were pooled and placed in pre-weighed and labeled Eppendorf tubes. Finally, all samples were oven-dried at 60 °C for 24 h and stored in a freezer at − 20 °C until Ag content analysis was performed by AAS. Results obtained were expressed in mg Ag kg^{-1} dry weight.

$$\mathrm{HPI} = \frac{\mathrm{HP\ weight}}{\mathrm{final\ shrimp\ weight}} \cdot 100 \qquad (2)$$

Depuration in vivo test The second in vivo test was conducted to evaluate Ag/AgCl NP depuration using feeds supplemented at 0 and 100 mg Ag kg^{-1} nominal concentrations. The protocol was designed according to OECD recommendations which set uptake and depuration phases (OECD 2012; Connolly et al. 2016). *Litopaneis vannnamei* juvenile shrimp provided by FITMAR, Sinaloa, Mexico (1.9 ± 0.20 g mean initial weight) were randomly allocated in nine rectangular 10-L fibreglass tanks (19 shrimps per tank, two treatments and three replicates). Organisms were maintained in the same conditions as the first test. During the uptake phase (first 7 days), the organisms were fed the low-dose experimental diet, while the depuration phase (next 14 days) started on day 8 of the assay by switching to a diet without NPs supplement (0 mg Ag kg^{-1}). The experiment duration was 21 days.

Tissue sampling for depuration test The hepatopancreas, gills and muscle tissue from three shrimps per tank were randomly selected and dissected with tweezers at 0, 7, 16 years and 21 days of the assay. Dissected samples were pooled and placed in pre-weighed and labeled Eppendorf tubes. Finally, all the samples were oven-dried at 60 °C for 24 h and stored in a freezer at − 20 °C until Ag content analysis was performed by AAS. Results obtained were expressed in mg Ag kg^{-1} dry weight.

Depuration parameters Depuration rate and assimilation efficiency were determined based on a simple two-compartment model. To calculate the depuration rate (k_2), a linear regression of ln(concentration) versus time was performed. The slope of the regression line is an estimate of k_2. The chemical

assimilation efficiency (%) (α, absorption of test substance across the gut) was calculated with the formula in Eq. 3:

$$\alpha = \frac{C_{0d} \cdot k_2}{I_g \cdot C_{food}} \cdot \frac{1}{1 - e^{-k_2 t}} \qquad (3)$$

where $C_{0,d}$ is the measured concentration in shrimp at time zero of the depuration phase (mg Ag kg^{-1} of shrimp), k_2 is the overall (not growth-corrected) depuration rate constant (day^{-1}), C_{food} is the measured concentration in food (mg Ag kg^{-1} feed), t is the duration of the feeding period (day), and I_g is the food ingestion rate constant adjusted for shrimp growth (g feed × shrimp^{-1} × day^{-1}). During the uptake phase, I_g can be calculated as shown in Eq. 4:

$$I_g = \frac{I \cdot W_0}{W_{end\ of\ uptake}} \qquad (4)$$

where I is the gram feed per gram shrimp per day, W_0 is the mean shrimp weight at the start of the experiment, and $W_{end\ of\ uptake}$ is the mean weight on the last day of exposure.

Once the assimilation efficiency (α) is obtained, the biomagnifiction factor (BMF) can be calculated by multiplying α by the ingestion rate constant (I_g) and dividing by the (overall) depuration rate constant (k_2). Estimation of the time (day) needed to reach the 50% depuration ($t_{1/2}$) of Ag/AgCl NPs was estimated using Eq. 5.

$$t_{1/2} = \frac{0.693}{k_2} \qquad (5)$$

Statistical analyses Two-way ANOVA was used to analyse the significance on in vitro (diffusion disc assay), and one-way ANOVAs were used for in vivo assays (growth performance parameters, and final concentration of Ag in each tissue after 7 days of consumption), followed by Tukey post hoc tests. A Dunett post hoc test was used for the hepatosomatic index data ($p < 0.05$). All analyses were carried out using Statistica 8.0 (TIBCO Software, USA).

Results

NP synthesis and characterization Reduction of Ag+ to Ag° in the sample was confirmed through a colour change from the initial colourless AgNO$_3$ solution to reddish-brown after reacting with AEU (Fig. 1a, b). The ultraviolet-visible (UV-vis) absorbance spectrum for a purified Ag/AgCl NPs suspension presents a surface plasmon of resonance (SPR) peak centred at 435 nm; meanwhile, no peak was observed in the AEU spectrum (Fig. 1c). The final Ag concentration in the purified Ag/AgCl NPs solution was 535 μg Ag mL^{-1}.
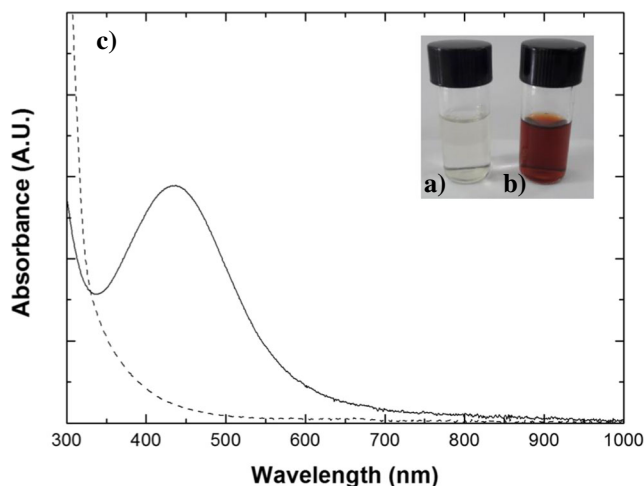
Fig. 1 (a) *Ulva* aqueous extract, (b) recently synthesized nanoparticles, (c) UV–vis absorption spectra of an Ag/AgCl NPs purified suspension (solid line) and *Ulva* aqueous extract (dash line) at room temperature

X-ray diffraction (XRD) studies The XRD spectrum of the Ag/AgCl NPs shows a pattern displaying diffraction peaks at around 27.7°, 32.1°, 46.1°, 54.8°, 57.4°, 67.5°, 74.5° and 76.7° (Fig. 2). These peaks show a good match with the reference peak positions of face-centred cubic (fcc) structure of silver chloride (space group Fm3m, Joint Committee on Power Diffraction Standard (JCPDS) file 31-1238). The most intense of these peaks, which is centred at 32.1°, is associated to the (200) planes of AgCl and has a corresponding mean coherence length value of $L_{200,AgCl} = 41(1)$ nm. In addition, less intense and rather wider peaks were found at approximately 38.1°, 44.3°, 64.4° and 77.5° and were associated to the (111), (200), (220) and (311) crystalline planes of fcc
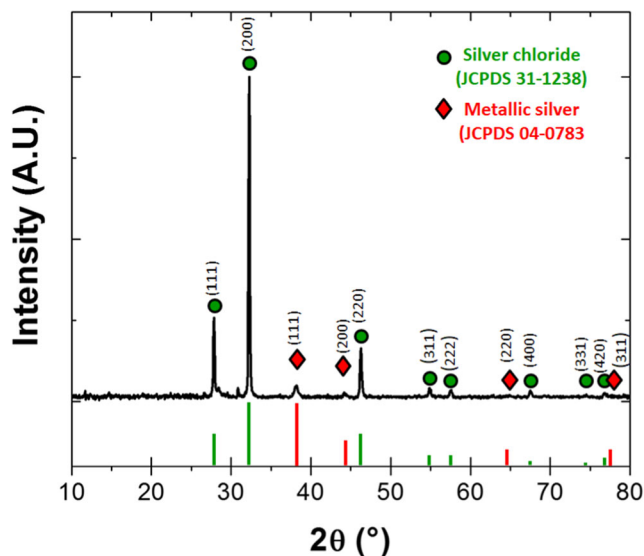
Fig. 2 XRD pattern of silver-based nanoparticles biosynthesized using an *Ulva* aqueous extract. Diffraction peaks match the reference positions of face-centred-cubic structures of AgCl (circles) or metallic Ag (diamonds)

metallic Ag structure, respectively (space group Fm3m, JCPDS file No. 04-0783). The average crystal size of this phase, estimated using the Scherrer equation and the position and width of the (111) peak, was $L_{111, Ag} = 18(1)$ nm.

Microstructural analyses Transmission electron microscopy (TEM) images (Fig. 3a) revealed that the sample was composed of spherical and irregular particles with different sizes, 90% being in the range from 5 to 20 nm and the rest of the particles from 20 to 35 nm. Consequently, the particle size distribution of the sample was fitted to a log-normal distribution. Particle size best-fitting central value and log-normal standard deviation were 9.5 and 0.44 nm, respectively (see insert image of Fig. 3a).

Selected area electron diffraction (SAED) patterns (Fig. 3b) exhibited spotty rings associated to both Ag and AgCl crystalline phases in agreement with the XRD results. Energy-dispersive X-ray (EDX) analysis (Fig. 3c) confirmed the presence of Ag, Cl and C in Ag/AgCl NPs (although the C peak partially comes from the lacey-carbon of the TEM grid). In addition, EDX spectrum often showed S peaks. The Cu peaks are due to background from the TEM grid. On the other hand, the presence of light elements, such as H, that are not detected using the EDX technique should not be discarded.

HRTEM images of the smallest nanoparticles (Figures S1a, S1c and S1e) displayed lattice fringes associated to a pure fcc Ag phase. Analysis of these micrographs by FFT (Figures S1b, S1d and S1f) revealed different microstructural characteristics in these particles, showing some to be polycrystalline (Figures S1a and S1e) with twinning boundaries and stacking faults (Figures S1e and S1f). However, nanoparticles with a rounded morphology and monocrystalline-like properties were also observed (Figures S1c and S1d), often along the [211] zone axis, and exhibited ½ {131} classically forbidden reflections.

The microstructural investigation of the largest particles by HRTEM (Figure S2a) revealed that they usually display both metallic Ag and AgCl crystals. An illustrative example is presented in Figures S2a–d. Figure S2a is an HRTEM image of two particles that display lattice fringes with d-spacing values associated to both crystalline phases detected by XRD and SAED, and that were determined analysing the spots of the corresponding FFT images (Figure S2b). Fourier filtering of HRTEM images selecting only reflections of AgCl (Figure S2c) or Ag (Figure S2d) showed the distribution of these crystalline phases in the particles, indicating that the crystals of both phases tend to coalesce to form particles of 20 to 35 of nanometres in size.

Fig. 3 **a**) Representative TEM image of Ag/AgCl NPs synthesized using *Ulva* aqueous extract. The insert image shows the related size distribution. Solid red line corresponds to the best log-normal distribution fit. **b**) SAED pattern. The expected positions of the diffraction rings associated to the crystallographic planes of fcc metallic silver (JCPDS 04-0783) and silver chloride (JCPDS 31-1238) are indicated. **c**) EDX spectrum
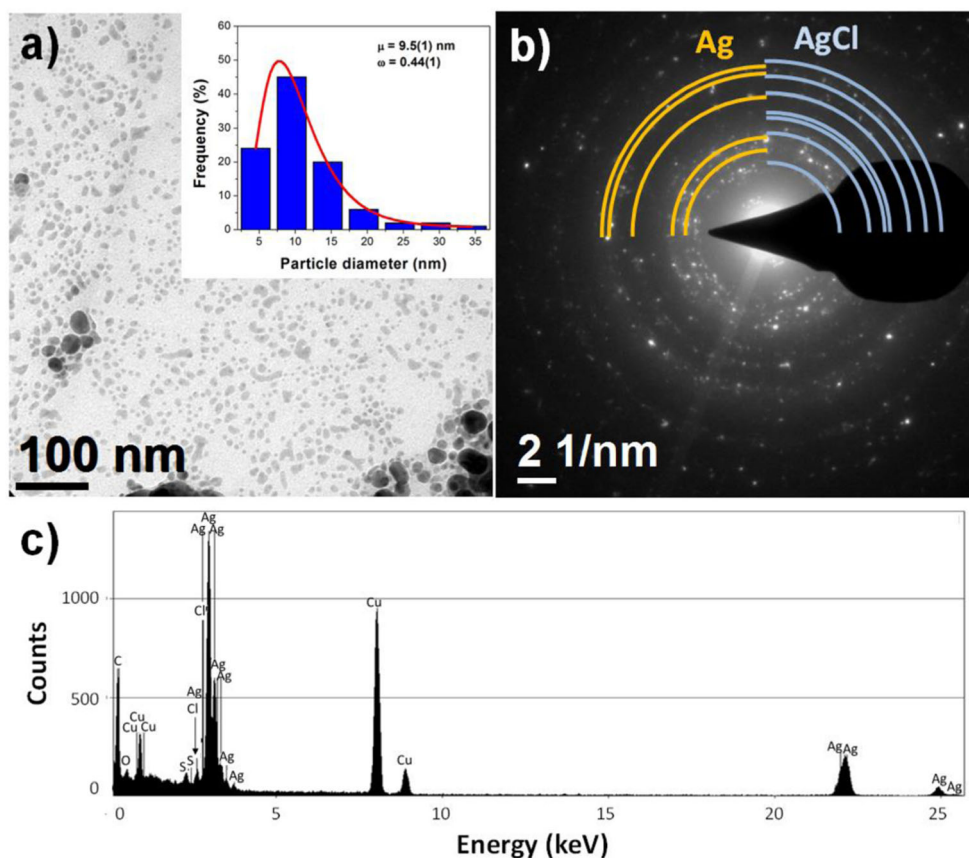
Fig. 4 FTIR spectra of (a) aqueous extract of *Ulva clathrata* and (b) Ag/AgCl NPs prepared using silver nitrate and the *Ulva clathrata* extract
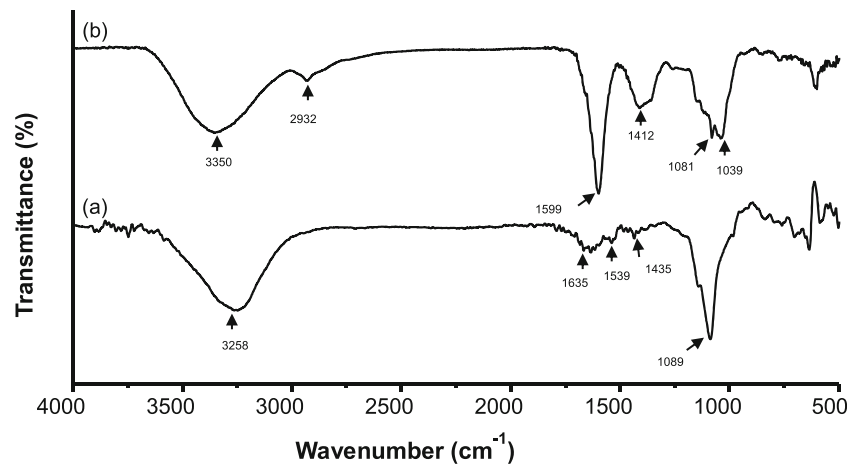
Fourier transform infrared spectrum (FTIR) In the FTIR spectrum of the AEU (Fig. 4a), the most significant FTIR bands were found at 3258 cm^{-1}, 1635 cm^{-1}, 1539 cm^{-1}, 1435 cm^{-1} and 1089 cm^{-1}. The broad band observed in the wavenumber range of $3700–2800 \text{ cm}^{-1}$ (centred at 3258 cm^{-1}) corresponded to O–H stretching vibrations from polysaccharides, polyphenols or proteins (Shanmugam et al. 2014). The peaks located at 1635 cm^{-1} and 1539 cm^{-1} were associated to the stretching vibration of the C=O group in peptides bound (amide I) and the N–H bending vibration (amide II) in proteins, respectively (Mendoza-Reséndez et al. 2013; Luna et al. 2015a, 2015b). The band located at 1435 cm^{-1} could potentially be due to C–N stretching vibration in amine or amide groups. The sharp and intense peak at 1089 cm^{-1} is due to C–N stretching vibration in aliphatic amines (Shanmugam et al. 2014) and C–O–C alcoholic groups associated with polysaccharides (Kora et al. 2012; Kannan et al. 2013b).

The Ag/AgCl NPs, after the purification process, presented major absorption bands at 3350 cm^{-1}, 2932 cm^{-1}, 1599 cm^{-1}, 1412 cm^{-1}, 1081 cm^{-1} and 1039 cm^{-1}. The broad band at 3350 cm^{-1}, ascribed to –O–H stretching vibrations, appeared shifted with respect to the same band observed in the spectrum of the algae extract. The band located at 2932 cm^{-1} can be ascribed to –C–H stretching vibrations in alkanes (Kora et al. 2012). In comparison with the FTIR spectrum of algae extract, an enhanced and shifted absorbance band appeared at 1599 cm^{-1}, suggesting modifications of the C=O and N–H stretching vibration in amine or amide groups due to these particles' involvement in the reduction process (Kannan et al. 2013b). The band at 1412 cm^{-1} could be ascribed to C–N stretching vibration of amine or amide groups. Also, the C–N stretching vibration band of aliphatic amines and C–O–C stretching vibration of alcoholic groups associated to polysaccharides (Kumar et al. 2012) appeared shifted at 1081 cm^{-1} and 1039 cm^{-1}, respectively.

Raman studies The Raman spectra of the algae extract used in the biosynthesis and the final product can be observed in Fig. 5. The spectrum of Ag-based particles displays highly pronounced bands at 228 cm^{-1}, 1370 cm^{-1} and 1595 cm^{-1} that are not observed in the algae extract spectrum. The sharp band at 228 cm^{-1} is attributed to stretching vibrations of Ag-N (Mukherjee et al. 2008; Kora et al. 2012) and Ag–O (Biswas et al. 2007; Kora et al. 2012) bonds, suggesting that proteins are bound to the particles' surface though amino and/or carboxylate (Kora et al. 2012). Moreover, intense bands at 1370 cm^{-1} and 1595 cm^{-1} were observed, which were associated to symmetric and asymmetric C=O stretching vibrations in the COO^- ions (Kora et al. 2012; Luna et al. 2015a, 2015b), respectively, and/or phenyl ring stretch (Biswas et al. 2007; Luna et al. 2015a, 2015b). Enhancement of the intensity of the C=O stretching vibrations bands indicates the direct binding of the COO^- group with the Ag surface (Kora et al. 2012).

Antibacterial activity

Disc diffusion assay The antibacterial test performed by disc diffusion showed significant differences in the growth inhibition zone diameter between the three *V. parahaemolyticus* strains ($p = 0.001$), for the products ($p = 0.001$) and in their
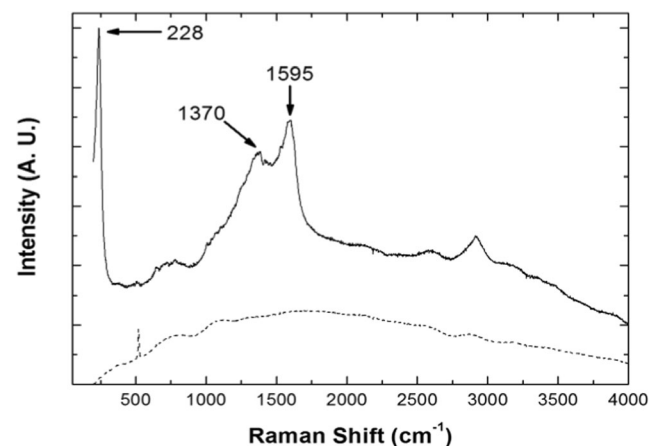
Fig. 5 Raman spectra of *Ulva clathrata* extract (dash line) and Ag/AgCl NPs (solid line)
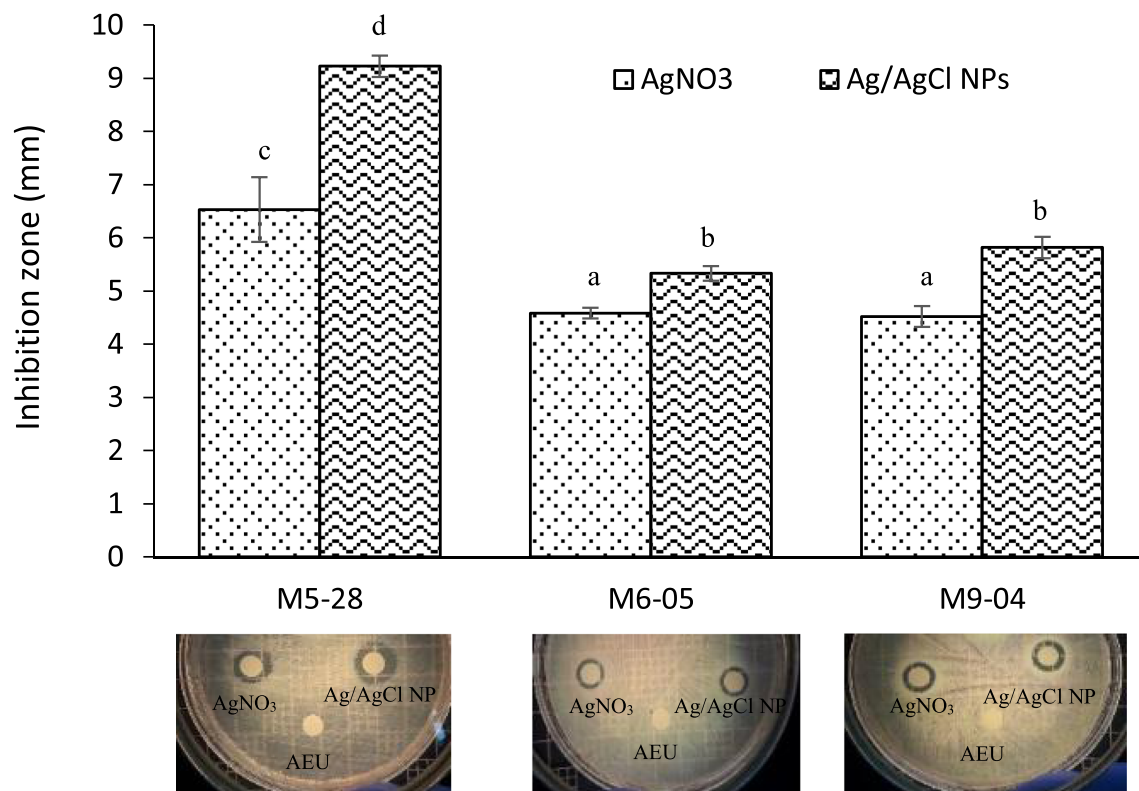
Fig. 6 Average inhibition zone diameters (mm) observed with diffusion method tested at similar concentrations (10 μg Ag per disc for Ag/AgCl NPs or AgNO$_3$). The error bars represent standard deviation (SD), and the data are means of three replicates ($n = 3$). The diameter of the paper disc is not included (6 mm). Different letters (a–d) represent significant differences according to a Fisher LSD post hoc multiple mean comparison test among the six treatments

interaction ($p = 0.001$) with a two-way ANOVA (Fig. 6). The discs impregnated with Ag/AgCl NPs produced an IZ of 9.2 ± 0.2, 5.3 ± 0.1 and 5.8 ± 0.2 mm for M5-28, M5-06 and M9-04 *V. parahaemolyticus* strains, respectively. The AgNO$_3$ solution tested at same concentration produced lower IZ than Ag/AgCl NPs, with values of 6.5 ± 0.6, 4.6 ± 0.1 and 4.5 ± 0.2 mm for the three strains, respectively. In contrast, the AEU did not cause inhibition.

Microdilution assay The antibacterial test performed by microdilution assay was only done with the products that had obtained an IZ on the disc diffusion assay. The Ag/AgCl NP solution presented a minimum inhibitory concentration (MIC) of 3.2 μg mL^{-1} for all strains tested, while the AgNO$_3$ solution showed a MIC of 1.6 μg mL^{-1} for *V. parahaemolyticus* M5-28 and M6-05 strains, and of 3.2 μg mL^{-1} for *V. parahaemolyticus* M9-04. The Ag/AgCl NP solution showed a minimum bactericide concentration (MBC) of 6.3 μg mL^{-1} for the three strains, while the AgNO$_3$ solution presented an MBC of 3.2 μg mL^{-1} for M5-28 and M6-05 strains, and of 6.3 μg mL^{-1} for M9-04 (Table 1).

Short-term evaluation in vivo test

Stability of nanoparticles in supplemented feed Ag contents in the experimental feeds are shown in Table 2. The leached

Table 1 In vitro antimicrobial activity of NPs vs AgNO$_3$ solutions as evidenced by microdilution assays ($n = 3$)

Vp strain	Ag/AgCl NPs		AgNO$_3$	
	MIC (μg mL^{-1})	MBC (μg mL^{-1})	MIC (μg mL^{-1})	MBC (μg mL^{-1})
M5-28	3.2	6.3	1.6	3.2
M6-05	3.2	6.3	1.6	3.2
M9-04	3.2	6.3	3.2	6.3

Minimum inhibitory concentration (MIC) and minimum bactericidal concentration (MBC)

Table 2 Concentrations of Ag in experimental diets and in water after leaching (means ± standard deviation, $n = 3$)

Theoretical concentrations[a]	Concentrations[a] in pellets before leaching	Concentrations[a] in pellets after leaching	Concentrations in water[b] after leaching
0	< 1	< 1	0.07 ± 0.03
10	12.73 ± 1.74	14.08 ± 0.75	0.14 ± 0.02
100	85.90 ± 4.58	90.75 ± 13.28	0.18 ± 0.09
1000	827.59 ± 50.96	936.77 ± 142.49	0.37 ± 0.19
10 000	9 971.10 ± 612.69	10 272.11 ± 483.34	5.01 ± 1.50

[a] mg Ag kg^{-1} dry matter

[b] mg Ag L^{-1}

feed had higher Ag content compared with the initial feed, and the nanoparticles lost from the feed surface to the seawater after 1 h were less than 5%.

Short-term acute toxicity in vivo (first test) and Ag distribution in tissues During the first short-term feed exposure test, the organisms showed no behavioural changes and survival was 100% for all treatments. The consumption of supplemented feed for 7 days did not cause significant changes in feed conversion but did affect weight gain (%), which was slightly improved in shrimp consuming feeds supplemented with 10 and 100 mg Ag kg^{-1} feed, and slightly (but not significantly) depressed in those consuming feeds with 10,000 mg Ag kg^{-1} (Table 3). In contrast, the hepatosomatic index (HPI) showed a significant reduction with the consumption of feeds supplemented with high doses (1000 and 10,000 mg Ag kg^{-1}; Fig. 7a).

Average concentration values of Ag were reported for different organ pools analysed at the end of 7 days of supplemented feed consumption (Fig. 1; hepatopancreas 7b, cephalothorax cuticle 7c and muscle 7d). A greater bioaccumulation of Ag was observed in hepatopancreas showing a dose-dependent relation of up to 1500 mg kg^{-1} dry weight (dw), while concentrations in cuticle and muscle were lower than 8 mg kg^{-1} dw. The hepatopancreas and cuticle Ag content became significantly different when diets contained 1000 and 10,000 ppm Ag. In contrast, muscle Ag contents did not change significantly with any treatment.

Depuration parameters (second test) The depuration rate (k_2), assimilation efficiency (α), half-life time ($t_{1/2}$) and biomagnification factor (BMF) could be determined for hepatopancreas and gills only (Fig. 8). The model used for calculating depuration parameters was not applicable in muscle

Table 3 Growth performance of *L. vannamei* juveniles fed for 7 days pelleted feeds supplemented with Ag/AgCl NPs at graded levels (from 0 to 10,000 mg Ag kg^{-1} feed, means ± standard deviation, $n = 3$)

Parameters	Experimental diets (mg Ag kg^{-1} feed)					p value
	0	10	100	1000	10,000	
Shrimp weight						
Mean initial body weight (g)	0.441 ± 0.012	0.444 ± 0.005	0.438 ± 0.002	0.438 ± 0.009	0.440 ± 0.002	0.851
Mean final body weight (g)	0.512 ± 0.010	0.540 ± 0.005	0.534 ± 0.013	0.508 ± 0.011	0.498 ± 0.023	0.232
Shrimp feed intake						
Mean feed offered (g feed g^{-1} shrimp day^{-1})	0.050 ± 0.00	0.050 ± 0.00	0.050 ± 0.00	0.050 ± 0.00	0.050 ± 0.00	1.000
Consumption of Ag/AgCl NPs (mg Ag g^{-1} shrimp day^{-1})	0.00[a]	0.64 ± 0.00[a]	4.3 ± 0.0[b]	41.4 ± 0.0[c]	499.0 ± 0.0[d]	< 0.001
Shrimp growth and feed response						
Weight gain (% WG)	16.1 ± 0.9	21.7 ± 1.0	21.9 ± 2.6	16.0 ± 2.1	13.1 ± 5.1	0.185
Feed conversion ratio (FCR)	5.0 ± 0.3	3.6 ± 0.2	3.8 ± 0.5	5.2 ± 0.8	8.1 ± 2.7	0.189
Shrimp survival (% S)	100	100	100	100	100	0.999

% WG = [(final mean weight − initial mean weight) / initial mean weight] × 100

FCR = total feed provided (g) / weight gain (g)

% S = (number of live organisms / initial number of organisms per tank) × 100

Superscript letters indicate different homogeneous subsets as determined by the Tukey multiple means comparison test
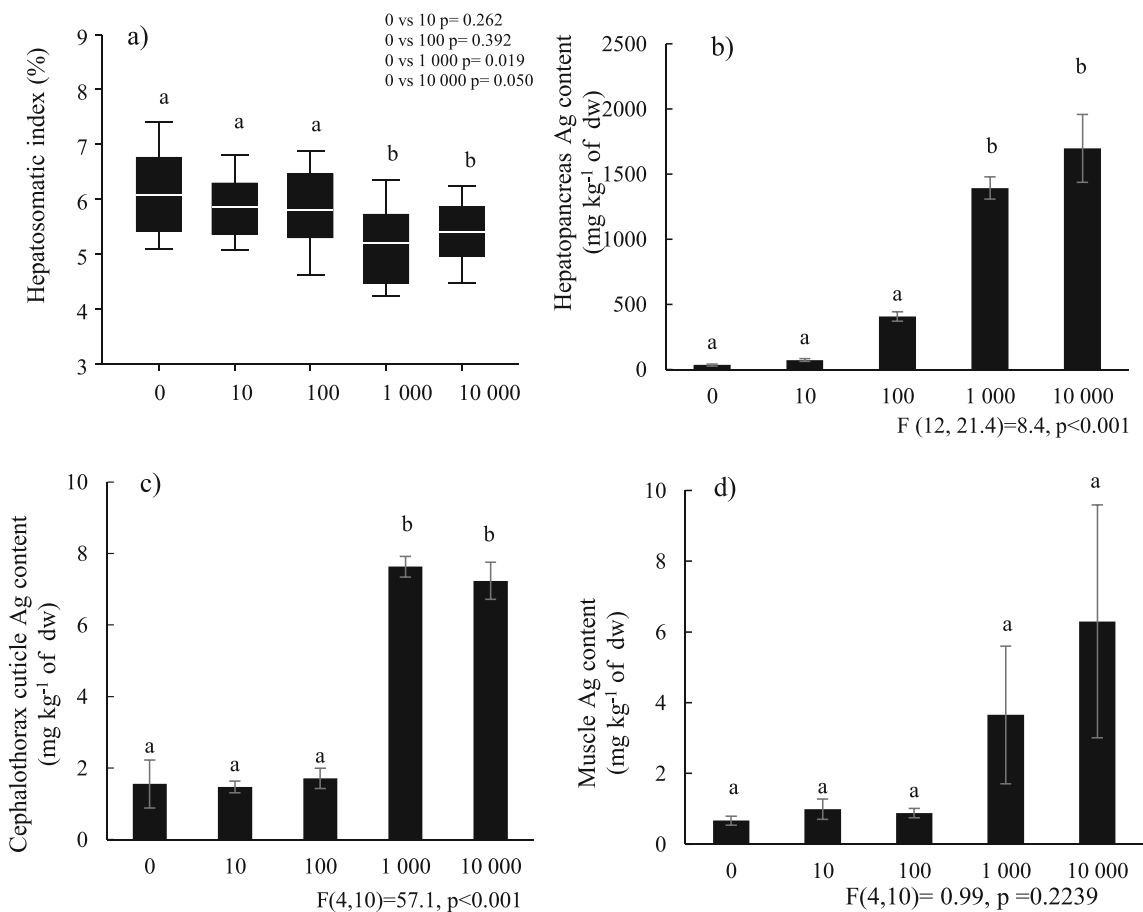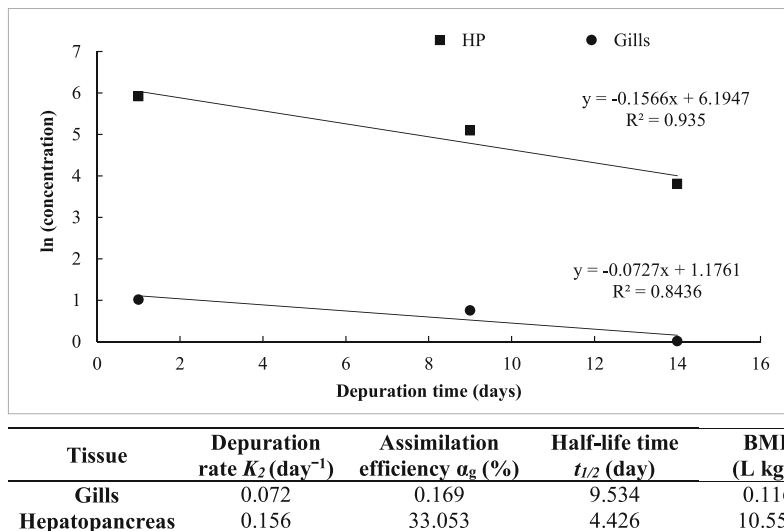
Fig. 7 **a**) Hepatosomatic index (HPI) box diagram ($n = 3$) and Ag bioaccumulation in shrimp tissues, **b**) hepatopancreas ($n = 12$), **c**) cephalothorax cuticle ($n = 4$) and **d**) muscle ($n = 4$) after consumption for 7 days of feeds supplemented with Ag/AgCl NPs at graded levels (from 0 to 10,000 mg Ag kg^{-1} feed). **a**) The white line represents the average HPI value ($n = 3$), letters on top of the bars indicate the absence (a) or presence (b) of a significant difference to the control group (Dunnet test). **b**)–**d**) Letters on top of the bars indicate different homogeneous subsets as determined by a Tukey multiple means comparison test. Error bars represent SD for all figures

tissue due to low Ag concentrations. However, results indicate that the hepatopancreas has higher k_2 and α values (0.156 day^{-1} and 33.053%, respectively) than gills (0.072 day^{-1} and 0.169%). The 50% depuration time (or $t_{1/2}$) was shorter in gills than in hepatopancreas, at 4.4 and 9.5 days, respectively. The hepatopancreas showed a high food biomagnification

Fig. 8 Kinetics of depuration model ln(concentration) of the Ag content in gills and hepatopancreas

Tissue	Depuration rate K_2 (day^{-1})	Assimilation efficiency α_g (%)	Half-life time $t_{1/2}$ (day)	BMF (L kg^{-1})
Gills	0.072	0.169	9.534	0.116
Hepatopancreas	0.156	33.053	4.426	10.553

factor (BMF) value of 10.553, while the gills had a 0.116 value. Finally, depuration of Ag accumulated in hepatopancreas and gills was already 89 and 99%, respectively, after only 14 days of depuration (i.e. consuming the feed without Ag/AgCl NPs).

Discussion

AgNPs exhibit an intense absorption peak in the UV-vis spectrum due to the SPR. According to Mie's theory, the form, width, height and the number of SPR peaks are strongly related with shape, particle size, concentration and distribution of the particles, respectively (Sun and Xia 2002; Dehnavi et al. 2013). The location and form of the single SPR peak observed for the purified Ag/AgCl NPs demonstrate the presence of spherical particles smaller than 100 nm, with a log-normal distribution. These results are in agreement with the SPR spectra reported by other authors for AgNPs or AgCl NPs (Choi et al. 2008; Mendoza-Reséndez et al. 2013; Dhas et al. 2014; Pal et al. 2015).

Ethanol is frequently used as an antisolvent to help recover the particles selectively (McLeod et al. 2005; Liu et al. 2009), in combination with centrifugation, in order to eliminate the ionic silver that had not reacted during the synthesis; additionally, centrifugation may be used to fraction particles by size (Novak et al. 2001; Pal et al. 2015). The final Ag concentration after the particle purification process was lower than the initial concentration due to elimination of Ag from the initial mixture.

The signals from the crystallographic planes on the XRD analysis indicate the presence of Ag and AgCl particles. The formation of these particles could be due to the interaction of the silver ions with chloride ions present in the *Ulva* extract. The presence of Na^+, K^+ and Cl^- is typical in macroalgae given that they are the main ions responsible for maintaining internal osmotic pressure (Lee and Liu 1999). Similar results have been reported by Dhas et al. (2014) and Venkatesan et al. (2016) regarding the biosynthesis of AgNPs with aqueous extracts of the brown algae *Sargassum plagiophyllum* and *Ecklonia cava.*

Synthesized NPs mediated by natural extracts also present special and unique morphological and microstructural characteristics, which are strongly linked to the reducing agent's composition. Ag/AgCl NPs exhibited a heterogeneous morphology, with a predominance of spherically and irregularly shaped particles. This is in agreement with reports from several authors of spherical, irregular and triangular particle shapes of NPs synthesized with green algae extracts (Yousefzadi et al. 2014; Sharma et al. 2016; Vijayan et al. 2016). Ag/AgCl NPs' sizes, as measured by TEM, are also similar to that of other AgNPs synthesized with green algae extracts. These authors report a range from 5 to 210 nm (Devi and Bhimba 2012; Kannan et al. 2013a; Abirami and

Kowsalya 2015; Sharma et al. 2016; Ramkumar et al. 2017). Particle size is relevant in this study given that the biological activity of NPs is strongly associated to their size distribution (Dehnavi et al. 2013).

Microstructural studies by SAED and EDX confirmed that particles are composed mostly of Ag and Cl, followed by C, S and O. These signals can likely be attributed to adsorbed proteins and sulphated polysaccharides (ulvan) coming from the extract composition. HRTEM studies exhibited two types of particles: The first are small, spherical and monocrystalline composed by only Ag phase, while the second are large, irregular and polycrystalline composed of Ag and AgCl phases. In addition, stacking faults were found in the morphology of large particles. This property and the irregular particle form are due to a growth in particle size by coalescence of smaller particles that seek to stabilize within the medium. This phenomenon has been reported briefly in AgNPs synthesized using natural extracts (Mendoza-Reséndez et al. 2013, 2014). There is only one previous report of gold particles with stacking faults. In that study, particles were synthesized using an aqueous extract of a unicellular green alga (*Chlorella vulgaris*), and the faults were attributed to particle growth and stabilization (Xie et al. 2007).

Seaweeds constitute an inexhaustible source of bioactive compounds and therefore are considered an important resource in biotechnology (Rauwel et al. 2015). Some biomolecules extracted from green algae, such as polysaccharides, peptides, phenolic compounds and pigments, are responsible for metal bioreduction during NP manufacture, because these compounds contain in their structure reducing functional groups like hydroxyl (–OH), carbonyl (–COOH), primary and secondary amines (–NH, –NH_2), alcohol and aldehydes (–CHO) (El-Kassas et al. 2014; Yousefzadi et al. 2014; Ramkumar et al. 2017). FTIR and Raman analyses confirmed the presence in the AEU of functional groups from biomolecules, mainly proteins, sulphated polysaccharides, and polyphenols that are adsorbed to the surface and microstructure of Ag/AgCl NPs. According to several authors who reported similar vibrations in FTIR studies of NPs synthesized with green algae extracts, these molecules are the main compounds responsible for reducing and buffering nanoparticles (El-Kassas et al. 2014; Ramkumar et al. 2017), making them more stable, and for a longer time, than those chemically synthesized (Vijayan et al. 2016). Additionally, these compounds may contribute novel and unique properties, as well as potential applications, for the corresponding NPs (Nezamdoost et al. 2014).

The antibacterial activity of the Ag/AgCl NPs obtained in the present study agreed with several authors who reported IZ with AgNPs or colloidal Ag in the range of 4.0 to 16.5 mm against *V. parahaemolyticus* AHPND[+] (Morales-Covarrubias et al. 2016; Sivaramasamy and Zhiwei 2016; Sivaramasamy et al. 2017) and 10 to 14.27 mm against *Vibrio harveyi* (Kandasamy et al. 2012; Sivaramasamy and Zhiwei 2016).

Sivaramasamy et al. (2017) reported similar results for AgNO$_3$ IZ ranging from < 1 to 4.6 mm for a strain of *V. parahaemolyticus* that causes AHPND (the diameter of the paper disc was not included for all results and comparisons in this paper). This result is interesting because Ag$^+$ ions arising from solutions of AgNO$_3$ usually exhibit more prominent effects in growth inhibition against bacteria than AgNPs (Choi et al. 2008). Some authors have reported antibacterial activity of *Ulva* sp. extracts (made with solvents of different polarities) against *Vibrio* and other important strains for human health (Rebecca et al. 2012; Saritha et al. 2013). However, in our case, AEU antibacterial activity was not observed. This result may be due to a difference in bacteria sensibility, *Ulva* species or the extraction method. Nevertheless, the compounds extracted with water from *U. clathrata* had an excellent reducing and stabilizing activity for the formation of NPs. Among the *V. parahaemolyticus* strains evaluated, M5-28 presented the highest susceptibility.

The minimum inhibitory concentration (MIC) represents the lowest concentration of antibacterial solution inhibiting bacterial growth. In contrast, the minimum bactericidal concentration (MBC) represents the lowest concentration of antibacterial solution required to kill more than 99.9% of the initial bacterial population (Petrus et al. 2011). The MIC and MBC values obtained for Ag/AgCl NP were below those reported by Petrus et al. (2011), where colloidal Ag was evaluated against other *Vibrio* strains reporting a MIC of 9.64 μg mL^{-1} and a MBC > 100 μg mL^{-1}. In contrast, MIC and MBC values for colloidal Ag against a strain of *Vibrio* causing AHPND reported by Morales-Covarrubias et al. (2016) were lower (2 μg mL^{-1}).

The differences between theoretical and measured Ag concentrations in supplemented feeds could be due to the manipulation during the preparation process, coupled with the analytical error. However, these differences with respect to nominal concentrations were acceptable. The increase shown in the Ag concentrations in feed after leaching can be attributed to the loss of soluble nutriments such as proteins (amino acids) and sugars, while less soluble ingredients, or those that do not leach in the water, were actually concentrated in the immersed feed. This result confirms that dietary exposure is a good and stable way to deliver NPs and to evaluate their effect in shrimp. Nevertheless, further studies regarding the residual content in shrimp feces and their final disposal are needed to inform future applications in shrimp aquaculture.

During the first in vivo test, consumption of feeds supplemented at low concentrations (10 and 100 ppm) had a positive effect on growth. This result coincides with survival and growth results reported by Sivaramasamy and Zhiwei (2016), who fed *L. vannamei* shrimp (6.82 ± 2.16 g) with a concentration of 10,000 ppm *Bacillus subtilis*-synthesized AgNPs for 65 days. In contrast, feeds supplemented at high concentrations (1000 and 10,000 ppm) likely resulted in moderate liver damage (non-visible), as suggested by a significant reduction in HPI. This negative effect on HPI, followed by histological damage, has been reported in trout after 8 weeks of being exposed to water with NPs at concentrations of 3300 and 1000 mg Ag L^{-1} (Monfared and Soltani 2013). However, there are no similar studies in shrimp allowing a comparison with our results in terms of HPI reduction and toxicity of dietary AgNPs.

In terms of bioaccumulation and biodistribution, the highest Ag concentrations found in hepatopancreas were not surprising, since the crustacean hepatopancreas gland can be considered a 'target organ' for the accumulation of many types of substances. In addition to performing important functions, such as secreting digestive enzymes, serving as the main site for food adsorption, and storing metabolic reserves, this organ also contains vesicles with metal-binding proteins that allow it to sequester heavy metals and other types of substances (Carvalho et al. 1999). In contrast, muscle showed practically no bioaccumulation, which is desirable given that it represents the most edible portion of the shrimp. However, medium-intensity bioaccumulation in the cephalothorax cuticle suggests that shell-on shrimp tails could contain certain levels of residual Ag. In this regard, several studies have found that the biodistribution and toxicity of nanoparticles are strongly influenced by particle size, shape, surface charge, surface coating and solubility (Sivaramasamy and Zhiwei 2016).

In addition, results suggest that shrimp have a fast Ag depuration capacity. This is mostly carried out by the hepatopancreas, which showed the highest depuration rates, similar to what was previously seen in the assimilation efficiency. The BMF value indicates how many times the Ag feed content can be biomagnified by hepatopancreas, which in this case indicates an Ag biomagnification capacity of ten times more than that administered by feed exposure.

Ag half-life times of 4 to 9 days were found in the tissues sampled during the depuration study (hepatopancreas, gills and muscle). This means that waiting an additional half-life period can eliminate 50% of the residual Ag. These values are lower than (but rather congruent with) that previously reported by Metian et al. (2010), who showed a *t*½ value of 10.8 ± 2 days for the depuration of *Litopenaeus stylirostris* after dietary exposure to radiolabeled Ag$^+$.

Several authors have studied the bioaccumulation and purification of noble and heavy metals including ionic, radiolabeled or complexed silver in crustaceans. Their purpose was to establish the current state of accumulation, distribution and migration within the trophic chain of metals that were a product of contamination in the ecosystem. The main objective of our study is not centered around metal contamination in aquatic systems but rather aims to provide information on next-generation antibacterial products manufactured using nanotechnology, and to promote appropriate doses that would have minimal impact on biological systems.

Conclusions

In vitro antibacterial activity studies herein suggest that Ag/AgCl NPs synthesized for the first time with aqueous extract of cultivated *U. clathrata* seaweed have a potential use for the management of Vp AHPND[+]. In addition, consumption of Ag/AgCl NPs through dietary exposure for 7 days had no lethal effects on shrimp. Finally, shrimp hepatopancreas has a rapid capacity for bioaccumulation and purification, while Ag accumulation was lower in cuticles and insignificant in muscle tissue. This suggests that headless, peeled shrimp could be safer than shell-on presentations. Results also indicate that Ag/AgCl NPs could be an effective treatment against AHPND[+] in farms. However, further studies are required to properly establish safe parameters when using Ag/AgCl NPs against *V. parahaemolyticus* AHPND[+] infections, as well as to investigate the specific effects of Ag/AgCl NPs on shrimp immune system and histology. Through additional research, we hope to provide a broader picture of the necessary considerations for the application of NPs as an antibacterial additive in shrimp feeds.

Author contributions statement MM-M synthetized the particles, performed the experiments, analysed the results and wrote the manuscript. CL conceived the synthesis and characterization of particles. RM-R conceived the synthesis and characterization of particles. EDB-C performed the characterization studies. SS-R provided the bacterial strains and conceived the microbiological studies. DR-M performed statistical and mathematical analyses, and wrote the manuscript. LEC-S designed and conceived all the experiments and wrote the manuscript. All authors reviewed the manuscript.

Compliance with ethical standards

Conflict of interest The authors declare that they have no conflict of interest.

References

Abdel-Raouf N, Al-Enazi NM, Ibraheem IBM (2017) Green biosynthesis of gold nanoparticles using *Galaxaura elongata* and characterization of their antibacterial activity. Arab J Chem 10:3029–3039

Abirami RG, Kowsalya S (2015) *Ulva fasciata* nanoparticles characterization and its anticancer activity. World J Pharm Pharm Sci 4:1164–1175

Aguirre-Guzmán G, Ruíz HM, Ascencio F (2004) A review of extracellular virulence product of *Vibrio* species important in diseases of cultivated shrimp. Aquac Res 35:1395–1404

AOAC (ed) (1997) Official Method of Analysis, 16th edn. AOAC International, Gaithersburg

Biswas N, Kapoor S, Mahal HS, Mukherjee T (2007) Adsorption of CGA on colloidal silver particles: DFT and SERS study. Chem Phys Lett 444:338–345

Carvalho RA, Benfield MC, Santschi PH (1999) Comparative bioaccumulation studies of colloidally complexed and free-ionic heavy metals in juvenile brown shrimp *Penaeus aztecus* (Crustacea: Decapoda: Penaeidae). Limnol Oceanogr 44:403–414

Choi O, Deng KK, Kim NJ, Ross L Jr, Surampallie RY, Hu Z (2008) The inhibitory effects of silver nanoparticles, silver ions, and silver chloride colloids on microbial growth. Water Res 42:3066–3074

Conapesca (2017) Anuario estadístico de acuacultura y pesca. Comisión Nacional de Acuacultura y Pesca, Mazatlan, Sinaloa, Mexico. pp 28 https://www.conapesca.gob.mx/work/sites/cona/dgppe/2017/ANUARIO_ESTADISTICO_2017.pdf. Access 26 Oct 2019

Connolly M, Fernández M, Conde E, Torrent F, Navas JM, Fernandez-Cruz ML (2016) Tissue distribution of zinc and subtle oxidative stress effects after dietary administration of ZnO nanoparticles to rainbow trout. Sci Total Environ 551–552:334–343

Cruz-Suarez LE, Tapia-Salazar M, Nieto-Lopez MG, Guajardo-Barbosa C, Ricque-Marie D (2009) Comparison of *Ulva clathrata* and the kelps *Macrocystis pyrifera* and *Ascophyllum nodosum* as ingredients in shrimp feeds. Aquac Nutr 15:421–430

Cruz-Suarez LE, León A, Peña-Rodríguez A, Rodríguez-Peña G, Moll B, Ricque-Marie D (2010) Shrimp/*Ulva* Co-Culture: A sustainable alternative to diminish the need for artificial feed and improve shrimp quality. Aquaculture 301:64–68

Cruz-Suarez LE, Nieto-Lopez M, Tapia-Salazar M, Maldonado-Muñiz M, Villarreal-Cavazos D, Ricque-Marie D (2013) Avances en la valoración de macroalgas del género *Ulva* como nutracéutico en *Litopenaeus vannamei*. In: Cruz-Suárez LE, Ricque-Marie D, Tapia-Salazar M, Nieto-Lopez MG, Villarreal-Cavazos DA, Gamboa-delgado J, Alvarez-Gonzalez C (eds) Contribuciones recientes en alimentacion acuicola. Universidad Autonoma de Nuevo León, San Nicolas de los Garza, pp 553–598 https://www.uanl.mx/utilerias/nutricion_acuicola/xii/LibroCRANA-ISBN.pdf. Access 08 July 2018

Defoirdt T, Sorgeloos P, Bossier P (2011) Alternatives to antibiotics for the control of bacterial disease in aquaculture. Curr Opin Microbiol 14:251–258

Dehnavi AS, Raisi A, Aroujalian A (2013) Control size and stability of colloidal silver nanoparticles with antibacterial activity prepared by a green synthesis method. Synth React Inorganic Met Nano-Metal Chem 43:543–551

Devi JS, Bhimba BV (2012) Anticancer activity of silver nanoparticles synthesized by the seaweed *Ulva lactuca In vitro*. J Nanomedine Biotherapeutic Discov 1:1–5

Dhas TS, Kumar VG, Karthick V, Jini AK, Govindaraju K (2014) Facile synthesis of silver chloride nanoparticles using marine alga and its antibacterial efficacy. Spectrochim Acta A 120:416–420

El-Kassas EK, El-Kassas H, E-K MM (2014) Biogenic silver nanoparticles using seaweed *Ulva rigida* and their fungicidal and cytotoxic effects. JKAU Mar Sci 25:3–20

Ibañez E, Herrero M, Mendiola JA, Castro-Puyana M (2012) Extraction and characterization of bioactive compounds with health benefits from marine resources: Macro and micro algae, cyanobacteria, and invertebrates. In: Hayes M (ed) Marine Bioactive Compounds: Sources, Characterization and Applications. Springer US, Boston, pp 55–98

Joshi J, Srisala J, Truong VH, Chen I-T, Nuangsaeng B, Suthienkul O, Lo CF, Flegel TW, Sritunyalucksana K, Thitamadee S (2014) Variation in *Vibrio parahaemolyticus* isolates from a single Thai shrimp farm

experiencing an outbreak of acute hepatopancreatic necrosis disease (AHPND). Aquaculture 428:297–302

Kandasamy K, Alikunhi NM, Manickaswami G, Nabikhan A, Ayyavu G (2012) Synthesis of silver nanoparticles by coastal plant *Prosopis chilensis* (L.) and their efficacy in controlling vibriosis in shrimp *Penaeus monodon*. Appl Nanosci 3:65–73

Kannan RRR, Arumugam R, Ramya D, Manivannan K, Anantharaman P (2013a) Green synthesis of silver nanoparticles using marine macroalga *Chaetomorpha linum*. Appl Nanosci 3:229–233

Kannan RRR, Stirk WA, Van Staden J (2013b) Synthesis of silver nanoparticles using the seaweed *Codium capitatum* P.C. Silva (Chlorophyceae). S Afr J Bot 86:1–4

Kora AJ, Sashidhar RB, Arunachalam J (2012) Aqueous extract of gum olibanum (*Boswellia serrata*): A reductant and stabilizer for the biosynthesis of antibacterial silver nanoparticles. Process Biochem 47:1516–1520

Kumar P, Selvi SS, Prabha AL, Kumar KP, Ganeshkumar RS, Govindaraju M (2012) Synthesis of silver nanoparticles from *Sargassum tenerrimum* and screening phytochemicals for its antibacterial activity. Nano Biomed Eng 4:12–16

Laramore S, Baptiste R, Wills PS, Hanisak MD (2018) Utilization of IMTA-produced *Ulva lactuca* to supplement or partially replace pelleted diets in shrimp (*Litopenaeus vannamei*) reared in a clear water production system. J Appl Phycol 30:3603–3610

Lee T-M, Liu C-H (1999) Correlation of decreased calcium contents with proline accumulation in the marine green macroalga *Ulva fasciata* exposed to elevated NaCl contents in seawater. J Exp Bot 50:1855–1862

Liu J, He F, Gunn TM, Zhao D, Roberts CB (2009) Precise seed-mediated growth and size-controlled synthesis of palladium nanoparticles using a green chemistry approach. Langmuir 25:7116–7128

Luna C, Cruz-Suarez LE, Mendoza-Resendez R, Ricque-Marie D, Gonzalez-Dueñas C, Maldonado-Muñiz M (2015a) Instituto Mexicano de la Propiedad Intelectual (IMPI) Solicitud de Patente MX/a/2015/002621 https://siga.impi.gob.mx/newSIGA/content/common/principal.jsf. Access 26 Oct 2019

Luna C, Chávez VHG, Barriga-Castro ED, Nuñez N, Mendoza-Resendez R (2015b) Biosynthesis of silver fine particles and particles decorated with nanoparticles using the extract of *Illicium verum* (star anise) seeds. Spectrochim Acta A 141:43–50

McLeod MC, Kitchens CL, Roberts CB (2005) CO_2-expanded liquid deposition of ligand-stabilized nanoparticles as uniform, wide-area nanoparticle films. Langmuir 21:2414–2418

Mendoza-Reséndez R, Núñez NO, Barriga-Castro ED, Luna C (2013) Synthesis of metallic silver nanoparticles and silver organometallic nanodisks mediated by extracts of *Capsicum annuum* var. *aviculare* (piquin) fruits. RSC Adv 3:20765–20771

Mendoza-Reséndez R, Gómez-Treviño A, Barriga-Castro ED, Nuñez N, Luna C (2014) Synthesis of antibacterial silver-based nanodisks and dendritic structures mediated by royal jelly. RSC Adv 4:1650–1658

Metian M, Hédouin L, Eltayeb MM, Lacoue-Labarthe T, Teyssié JL, Mugnier C, Bustamante P, Warnau M (2010) Metal and metalloid bioaccumulation in the Pacific blue shrimp *Litopenaeus stylirostris* (Stimpson) from New Caledonia: Laboratory and field studies. Mar Pollut Bull 61:576–584

Monfared AL, Soltani S (2013) Effects of silver nanoparticles administration on the liver of rainbow trout (*Oncorhynchus mykiss*): histological and biochemical studies. Pelagia Res Libr 3:285–289

Morales-Covarrubias MS, García-Aguilar N, Bolan-Mejía MDC, Puello-Cruz AC (2016) Evaluation of medicinal plants and colloidal silver efficiency against *Vibrio parahaemolyticus* infection in *Litopenaeus vannamei* cultured at low salinity. Dis Aquat Org 122:57–65

Mukherjee P, Roy M, Mandal BP, Dey GK, Mukherjee PK, Ghatak J, Tyagi AK, Kale SP (2008) Green synthesis of highly stabilized nanocrystalline silver particles by a non-pathogenic and agriculturally important fungus *T. asperellum*. Nanotechnology 19:1–7

Nezamdoost T, Bagherieh-Najjar MB, Aghdasi M (2014) Biogenic synthesis of stable bioactive silver chloride nanoparticles using *Onosma dichroantha* Boiss. root extract. Mater Lett 137:225–228

Nieto-López M, Tapia-Salazar M, Ricque-Marie D, Villarreal-Cavazos D, Lemme A, Cruz-Suárez LE (2011) Digestibility of different wheat products in white shrimp *Litopenaeus vannamei* juveniles. Aquaculture 319:369–376

Novak JP, Nickerson C, Franzen S, Feldheim DL (2001) Purification of molecularly bridged metal nanoparticle arrays by centrifugation and size exclusion chromatography. Anal Chem 73:5758–5761

OECD (2005) OECD Detailed review paper on aquatic arthropods in life cycle and two-generation toxicity tests. OECD Environment Health and Safety Publications, OECD Publishing, Paris, http://www.oecd.org/chemicalsafety/testing/34241659.pdf. Accessed 15 Feb 2017

OECD (2012) Test No. 305: Bioaccumulation in Fish: Aqueous and Dietary Exposure, OECD Guidelines for the Testing of Chemicals, Section 3, OECD Publishing, Paris https://doi.org/10.1787/9789264185296-en

OIE (2014)Antimicrobial use in aquatic animals. In: Aquatic animal health code, Seventeent. World organisation for animal health, Paris, pp 109-117

Pal S, Tak YK, Song JM (2015) Does the antibacterial activity of silver nanoparticles depend on the shape of the nanoparticle? A study of the Gram-negative bacterium *Escherichia coli*. J Biol Chem 290:1712–1720

Peña-Rodríguez A, León A, Moll B, Tapia-Salazar M, Nieto-López MG, Villarreal-Cavazos D, Ricque-Marie D, Cruz-Suárez LE (2010) Uso de Ulva clathrata en la nutrición del camarón blanco: revisión. En: Cruz-Suarez LE, Ricque-Marie D, TapiaSalazar M, Nieto-López MG, Villarreal-Cavazos A, Gamboa-Delgado J (Eds), Avances en Nutrición Acuícola X - Memorias del X Simposio Internacional de Nutrición Acuícola, 8-10 de Noviembre, San Nicolás de los Garza, N. L., México.Universidad Autónoma de Nuevo León, Monterrey, México, pp 700–712

Peña-Rodríguez A, Mawhinney TP, Ricque-Marie D, Cruz-Suárez LE (2011) Chemical composition of cultivated seaweed *Ulva clathrata* (Roth) C. Agardh. Food Chem 129:491–498

Petrus EM, Tinakumari S, Chai LC, Ubong A, Tunung R, Elexson N, Chai LF, Son R (2011) A study on the minimum inhibitory concentration and minimum bactericidal concentration of nano colloidal silver on food-borne pathogens. Int Food Res J 18:55–66

Prasad TNVKV, Kambala VSR, Naidu R (2013) Phyconanotechnology: synthesis of silver nanoparticles using brown marine algae *Cystophora moniliformis* and their characterisation. J Appl Phycol 25:177–182

Rai M, Yadav A, Gade A (2009) Silver nanoparticles as a new generation of antimicrobials. Biotechnol Adv 27:76–83

Ramkumar VS, Pugazhendhi A, Gopalakrishnan K, Sivagurunathan P, Saratale GD, Dung TNB, Kannapiranf K (2017) Biofabrication and characterization of silver nanoparticles using aqueous extract of seaweed *Enteromorpha compressa* and its biomedical properties. Biotechnol Rep 14:1–7

Rauwel P, Küünal S, Ferdov S, Rauwel E (2015) A review on the green synthesis of silver nanoparticles and their morphologies studied via TEM. Adv Mater Sci Eng 2015:1–9

Rebecca LJ, Dhanalakshmi V, Sharmila S (2012) Effect of the extract of *Ulva* sp on pathogenic microorganisms. J Chem Pharm Res 4:4875–4878

Saritha K, Mani AE, Priyalaxmi M, Patterson J (2013) Antibacterial activity and biochemical constituents of seaweed *Ulva lactuca*. Glob J Pharmacol 7:276–282

Sarker SD, Nahar L, Kumarasamy Y (2007) Microtitre plate-based antibacterial assay incorporating resazurin as an indicator of cell growth, and its application in the *in vitro* antibacterial screening of phytochemicals. Methods 42:321–324

Shanmugam N, Rajkamal P, Cholan S, Kannadasan N, Sathishukumar K, Viruthagiri G, Sundaramanickam A (2014) Biosynthesis of silver nanoparticles from the marine seaweed *Sargassum wightii* and their antibacterial activity against some human pathogens. Appl Nanosci 4:881–888

Sharma A, Sharma S, Sharma K, Chetri S, Vashishtha A, Singh P, Kumar R, Rathi B, Agrawa V (2016) Algae as crucial organisms in advancing nanotechnology: a systematic review. J Appl Phycol 28:1759–1774

Singh CR, Kathiresan K, Anandhan S (2015) A review on marine based nanoparticles and their potential applications. Afr J Biotechnol 14: 1525–1532

Sirvakumar K, Kannappan S, Masilamani D, Prasanna KP (2014) Evaluation of marine macro alga, *Ulva fasciata* against bioluminescent causing *Vibrio harveyi* during *Penaeus monodon* larviculture. Afr J Microbiol Res 8:803–813

Sivaramasamy E, Zhiwei W (2016) Enhancement of vibriosis resistance in *Litopenaeus vannamei* by supplementation of biomastered silver nanoparticles by *Bacillus subtilis*. J Nanomed Nanotechnol 7:1–10

Sivaramasamy E, Zagorsek K, Li F, Xiang J (2017) In situ synthesis of silver nanoparticles into TEMPO-mediated oxidized bacterial cellulose and their antivibriocidal activity against shrimp pathogens. Carbohydr Polym 166:329–337

Soto-Rodriguez SA, Gomez-Gil B, Lozano-Olvera R, Betancourt-Lozano M, Morales-Covarrubias MS (2015) Field and experimental evidence of *Vibrio parahaemolyticus* as the causative agent of acute hepatopancreatic necrosis disease of cultured shrimp (*Litopenaeus vannamei*) in Northwestern Mexico. Appl Environ Microbiol 81: 1689–1699

Sun Y, Xia Y (2002) Shape-controlled synthesis of gold and silver nanoparticles. Science 298:2176–2179

Swain P, Sasmal A, Nayak SK, Barik S, Mishra SS, Mohapatra KD, Swain SK, Saha JN, Sen AK, Jayasankar P (2014) Evaluation of selected metal nanoparticles on hatching and survival of larvae and fry of Indian major carp, rohu (*Labeo rohita*). Aquac Res 47:498–511

Venkatesan J, Kim S-K, Shim M (2016) Antimicrobial, antioxidant, and anticancer activities of biosynthesized silver nanoparticles using marine algae *Ecklonia cava*. Nanomaterials 6:1–18

Vieira AP, Stein EM, Andreguetti DX, Colepicolo P, da Costa Ferreira AM (2016) Preparation of silver nanoparticles using aqueous extracts of the red algae *Laurencia aldingensis* and *Laurenciella* sp. and their cytotoxic activities. J Appl Phycol 28:2615–2622

Vijayan SR, Santhiyagu P, Ramasamy R, Aravalagan P, Kumar G, Ethiraj K, Ramaswamy BR (2016) Seaweeds: A resource for marine bionanotechnology. Enzym Microb Technol 95:45–57

Xie J, Lee JY, Wang DIC, Ting YP (2007) Identification of active biomolecules in the high-yield synthesis of single-crystalline gold nanoplates in algal solutions. Small 3:672–682

Yang YT, Chen IT, Lee CT, Chen CY, Lin SS, Hor LI, Tseng TC, Huang YT, Sritunyalucksana K, Thitamadee S, Wang HC, Lo CF (2014) Draft genome sequences of four strains of *Vibrio parahaemolyticus*, three of which cause Early Mortality Syndrome/Acute Hepatopancreatic Necrosis Disease in shrimp in China and Thailand. Genome Announc 2:e00816–e00814

Yousefzadi M, Rahimi Z, Ghafori V (2014) The green synthesis , characterization and antimicrobial activities of silver nanoparticles synthesized from green alga *Enteromorpha flexuosa* (Wulfen). J Agardh Mater Lett 137:1–4

Zhao G, Stevens SE (1998) Multiple parameters for the comprehensive evaluation of the susceptibility of *Escherichia coli* to the silver ion. BioMetals 11:27–32